Journal of ELECTRONIC MATERIALS, Vol. 48, No. 7, 2019
https://doi.org/10.1007/s11664-019-07218-2

Growth and Characterization of a Nonlinear Optical Material: L-Histidine-Doped Imidazolinium L-Tartrate

P. DHIVYA,[1] R. ARUN KUMAR,[1,2,5,6] T. THEIVASANTHI,[3] G. VINITHA,[4] and M.D. KANNAN[2]

1.—GRD Centre for Materials Research, PSG College of Technology, Coimbatore 641 004, India. 2.—Department of Physics, PSG College of Technology, Coimbatore, India. 3.—International Research Centre, Kalasalingam University, Krishnankoil, India. 4.—Division of Physics, School of Advanced Studies, Vellore Institute of Technology, Chennai, India. 5.—e-mail: rarunpsgtech@yahoo.com. 6.—e-mail: rak@phy.psgtech.ac.in

Imidazolinium L-tartrate (IMLT) crystals and L-histidine-doped IMLT crystals were grown by slow evaporation technique at room temperature. The powder x-ray diffraction technique confirms the lattice parameters and shifts in the peak positions attributed to the dopant L-histidine. The Fourier transform infrared (FTIR) spectrum reveals the assignments of characteristic bondings present in the grown crystals. The frequency-dependent dielectric constant and dielectric loss of pure and L-histidine-doped IMLT crystals have been investigated by the dielectric measurements. Doping has improved the optical parameters and was studied using UV–Vis-near infrared (NIR) spectral studies. The cut-off wavelengths of pure and 1 mol.% L-histidine-doped IMLT crystals were observed at 234 nm and 229 nm, respectively. The etching study examines the growth mechanism and surface morphology of the pure and L-histidine-doped IMLT crystals. The carbon-hydrogen-nitrogen (CHN) analysis conveys the percentage of carbon, hydrogen and nitrogen elements present in pure and L-histidine-doped IMLT crystals. The consequences of doping L-histidine in IMLT single crystal and their dominance in various properties of the crystal grown in aqueous solution by slow evaporation technique have been explored.

Key words: Imidazolinium L-tartrate, powder XRD, optical studies, dielectric studies, *Z*-scan technique

INTRODUCTION

The strong demand for single crystals with favourable physical and chemical properties has led to the development of research in materials science. Crystals with superior perfection have potential use in optical device applications, telecommunications and information processing. Nonlinear optical (NLO) materials exhibiting high performance are used as components in frequency conversion techniques, optical communications, electro-optical modulators, etc.[1] Among the NLO materials, organic compounds possess more favourable physical properties, such as crystallization with hydrogen bonds, weak Van der Waal force (large dipole moment), large birefringence and high optical damage threshold for laser power.[2] The delocalized π-electron system of an aromatic heterocyclic compound increases the molecular hyperpolarizability which is essential for enhancing the NLO property of the crystal.

Imidazole ($C_3H_4N_2$) is an organic compound with a π-bonded system. Due to the overlap of π-orbitals, delocalization of electronic charge distribution leads to high mobility in the electron density.[3] L-tartaric acid ($C_4H_6O_6$), a small organic molecule capable of initiating multidirectional hydrogen bonding with large dipole moment and wide transparency range,

(Received August 9, 2018; accepted April 11, 2019; published online April 24, 2019)

is combined with imidazole to synthesize a second-order NLO active material, imidazolinium L-tartrate (IMLT). IMLT is a bulk organic crystal with an excellent laser damage threshold (7.45 GW cm^{-2}) as compared to Potassium di hydrogen ortho phosphate and Beta-barium borate (5 GW cm^{-2}) which was found using a high-power xenon laser with energy of 400 mJ and a diameter 0.86 mm.[4] Amino acids are organic compounds with relatively high melting points, with a deprotonated carboxylic acid (COO^-) group and a protonated amino group (NH_3^+).[5] The dipolar nature enhances the chemical stability and transparency of the host material, thus making them ideal candidates for NLO applications. Almost all amino acids contain an asymmetric carbon atom; i.e., they exhibit molecular chirality and crystallize in a noncentrosymmetric space group. L-histidine ($C_6H_9N_3O_2$) is a polar, basic amino acid which is doped in IMLT to enhance its molecular hyper-polarizability. The molecular structure of L-histidine and imidazole are similar, as shown in Fig. 1; however, L-histidine is an amino acid containing an electron donor and acceptor group, and has molecular chirality and a zwitterionic nature, which are the characteristic properties of all amino acids.[6] These properties enhance the nonlinear optical behaviour, thereby facilitating the growth of good-quality crystals with better optical properties than the undoped crystals. The pure IMLT and L-histidine-doped IMLT crystals can be utilized in the electro-optical modulator and optical power limiting applications.[7] In this present work, pure IMLT and L-histidine-doped IMLT crystals were synthesized and subjected to various characterization analyses. The effects of addition of dopants have successfully promoted the NLO properties of various crystals. Amino acid triggers the extensive hydrogen bonding, and enhances the charge delocalization of the parent molecule through a donor–acceptor group. The dopants offer better acentric molecular alignment to the parent molecule. Also, dopants occupy either the vacancies or interstitial positions in the parent molecule, which suppresses the defects, cracks and impurities.

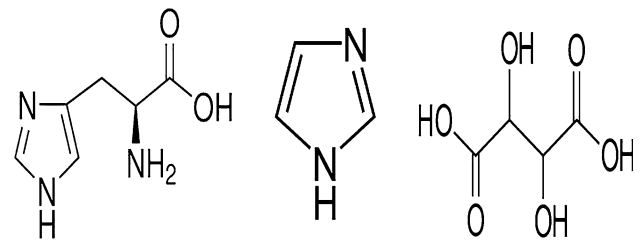

Fig. 1. Structure of L-histidine, imidazole and L-tartaric acid.

EXPERIMENT

Material Synthesis and Crystal Growth

There are different methods available for the growth of single crystals—melt growth, slow evaporation, slow cooling, vapour growth, etc.[8] among which the slow evaporation technique was chosen for the growth of IMLT single crystals because of its simplicity in growth procedure and to reduce the complications in equipment. An equimolar ratio of imidazole and L-tartaric acid was made for dissolution in deionized water by stirring continuously for 6 h to obtain a homogeneous solution.

The saturated solution was filtered in a clean beaker using Whatman filter paper to remove the impurities. Then a perforated sheet was used to cover the beaker and kept for slow solvent evaporation. Within 1 day, the nucleation was observed. A number of tiny crystals were grown in a period of 7 days. Photographs of the crystals obtained are shown in Fig. 2. A perfect seed crystal was selected and suspended using a nylon thread in the mother solution for further growth of the bulk IMLT crystal. Doping of L-histidine was achieved by adding the material at 1 mol.%, 3 mol.% and 5 mol.% in pure IMLT solution, and the same procedure was adopted to grow L-histidine-doped IMLT single crystals. A photograph of the bulk crystals is shown in Fig. 3. High-quality transparent crystals were grown in lower concentrations of dopants. Fewer occlusions may occur in higher concentrations of doped crystals.

RESULTS AND DISCUSSION

Powder X-ray Diffraction

The powder x-ray diffraction (PXRD) analysis of pure and L-histidine-doped IMLT single crystals were recorded using a Bruker D8 Advance powder x-ray diffractometer with CuKα radiation of wavelength 1.5406 Å (40 kV, 20 mA) in the angular range (2θ) 10°–50° to analyse the crystal system and lattice parameters. The recorded PXRD patterns are shown in Fig. 4. The grown crystal belongs to the monoclinic crystal system with the space group $P2_1$. Various planes of reflection were observed in the figure, and the resulting pattern reveals that there is no phase change, showing the absence of any additional peaks due to doping of L-histidine. Sharp, high, intense peaks demonstrate the superior crystallinity of the grown crystals.[9] The PXRD pattern reveals that the diffraction pattern consists of only the original peaks of pure IMLT, which clearly shows that the L-histidine dopant has not changed the phases of IMLT crystal; furthermore, there is no complex crystal formation.[9] The unit cell parameters of L-histidine-doped IMLT crystals have slightly changed with reference to the pure IMLT, which should have occurred due to the strain enforced on lattice sites of pure IMLT crystal by the dopant L-histidine. In the PXRD pattern of pure and

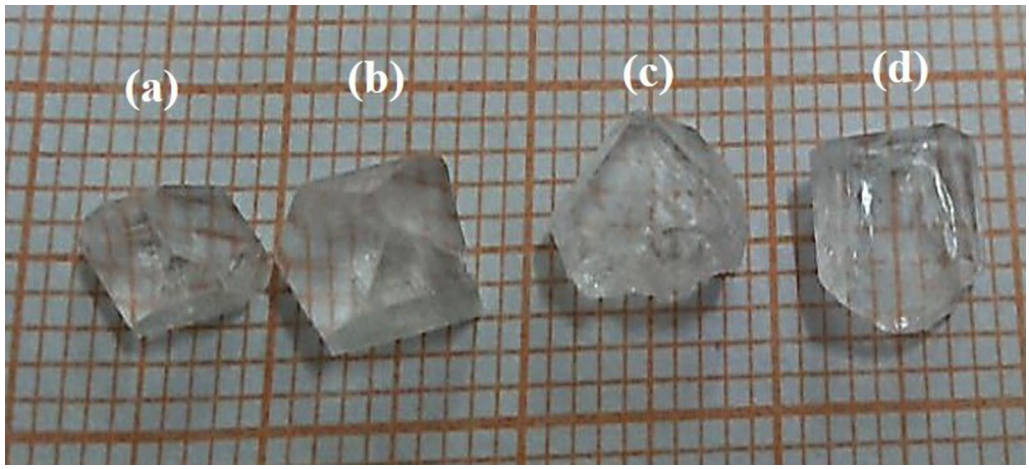

Fig. 2. Photograph of crystals of (a) pure IMLT (b) 1 mol.% (c) 3 mol.% and (d) 5 mol.% L-histidine-doped IMLT.

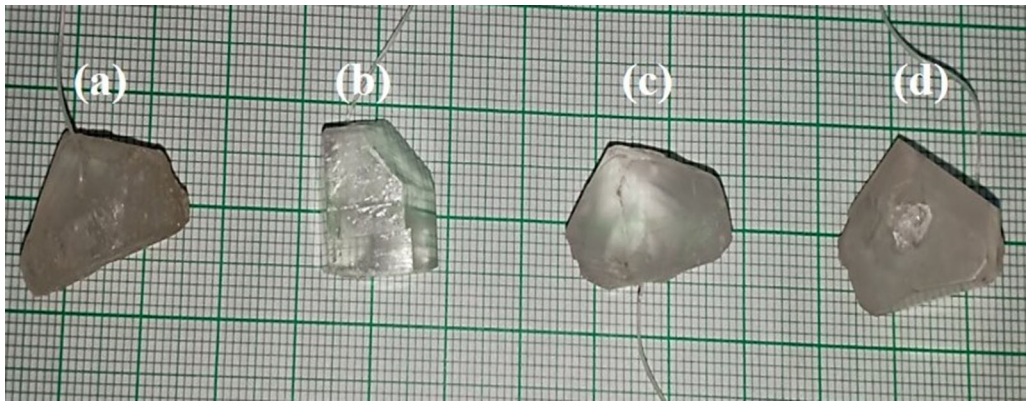

Fig. 3. The photograph of (a) pure IMLT (b) 1 mol.% L-histidine (c) 3 mol.% L-histidine and (d) 5 mol.% L-histidine-doped IMLT bulk crystals.

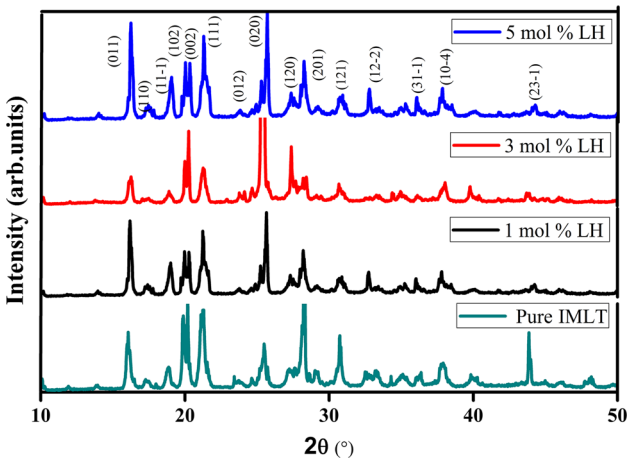

Fig. 4. PXRD patterns of pure IMLT and L-histidine-doped IMLT crystals.

L-histidine-doped IMLT crystals, (020), (011) and (111) planes are the most prominent peaks with maximum intensity. Conversely, the intensity of a few reflections of the planes (201), (121) and (23-1) were found to decrease. These observations could be attributed to the formation of lattice strains. The increase in cell volume and the deviation in the lattice parameters are shown in Table I. It is observed that by increasing the concentration of the dopant, the strain produced in the crystal lattice is tensile in nature. The variation in the cell volume depends on the positional occupancy of the dopant. Here, the dopant enters into the IMLT crystalline matrix occupying typically the interstitial position without causing much distortion in the grown crystal. However, the properties of the crystals such as thermal, optical, chemical and mechanical properties are bound by its nature of crystallinity. The size of the crystallites expresses the increase in the crystallinity of a compound. The sharpness in the peak of the PXRD pattern is owing to the increase in the crystallinity.[10,11]

By using the Debye–Scherrer formula, the crystallite sizes, corresponding to the (011) (020) and (111) planes, were calculated, and the average value is furnished in Table II. The study of the dislocation density unveils the measure of the crystal quality.[8]

Table I. Parameters of pure IMLT and L-histidine-doped IMLT crystals

Lattice parameters	Pure IMLT	1 mol.% L-histidine-doped IMLT	3 mol.% L-histidine-doped IMLT	5 mol.% L-histidine-doped IMLT
a (Å)	6.78	6.83	6.78	6.88
b (Å)	6.92	6.95	7.04	7.06
c (Å)	9.67	9.60	9.61	9.79
β (°)	87.40	87.61	87.79	89.26
$\alpha = \gamma$ (°)	90	90	90	90
Cell volume (Å)^3	454.02	461.51	474.46	483.05
Crystal structure	Monoclinic	Monoclinic	Monoclinic	Monoclinic

Table II. Representation of crystallite size (D), strain (ε) and dislocation density (δ) of the grown crystals

Crystal	Crystallite size (D) × 10^{-8} m	Strain (ε) (lin^{-2} m^{-3}) × 10^{-4}	Dislocation density (δ) (lin m^{-2})
Pure IMLT	1.99	17.42	1.94×10^{15}
1 mol.% L-histidine	5.55	6.24	2.42×10^{14}
3 mol.% L-histidine	4.32	8.03	3.99×10^{14}
5 mol.% L-histidine	3.10	11.15	7.82×10^{14}

Crystallite size (D), strain (ε) and dislocation density (δ) were calculated using the following relations:

$$D = \frac{K\lambda}{\beta \cos\theta} \quad (1)$$

$$\varepsilon = \frac{\beta \cos\theta}{4} \quad (2)$$

$$\delta = \frac{15\varepsilon}{(a \times D)} \quad (3)$$

where λ is the wavelength of the x-ray beam used, β is the full width at half maximum (in radians), K is the Scherrer constant and θ is the Bragg's diffraction angle. From Table II, it is observed that the 1 mol.% L-histidine-doped IMLT crystal has the lowest dislocation density (δ) and also the large crystallite size (D) compared to 3 and 5 mol.% L-histidine-doped IMLT crystals. This confirms the good crystallinity of the 1 mol.% L-histidine-doped IMLT crystal. Figure 5 represents the PXRD pattern of the 3 mol.% L-histidine-doped IMLT crystal, in which the pattern remains the same as pure IMLT, whereas the intensity of the peak corresponding to the (020) plane increases and has attained the maximum intensity. This may be due to the enlargement of the surface of (010) planes attributed to the faster growth of planes normal to it in the presence of 3 mol.% L-histidine dopant.[11] This indicates that the dopant molecules affect the morphology of the pure IMLT single crystal to a certain limit and does not change the crystal structure.

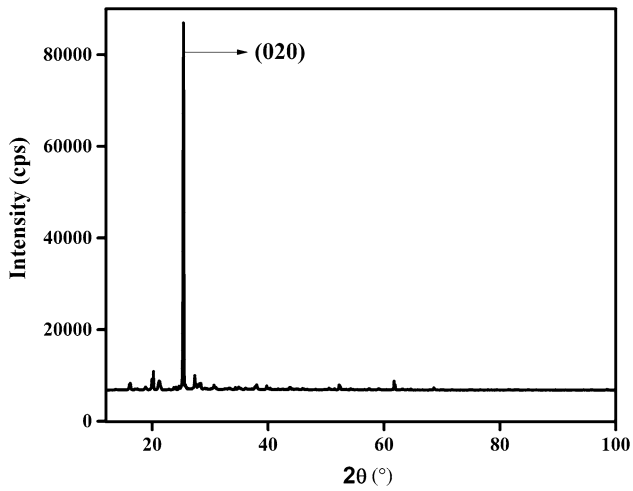

Fig. 5. PXRD pattern of 3 mol.% L-histidine-doped IMLT.

Optical Studies

The UV–Vis-NIR transmission spectra of pure and L-histidine-doped IMLT crystals were recorded in the wavelength region 200–2000 nm using a Varian Cary 5000 UV–Vis-NIR absorption spectrometer and are shown in Fig. 6. The grown crystals were found to be transparent in the entire UV, visible and NIR regions, which is due to the migration of electrons from the ground state to the higher-energy levels in σ-, π- and n-orbitals. At 1420 nm, the sharp narrow decrease in transmittance is attributed to the overtone of C–H vibration modes followed by a distinct absorption band from 2000 nm which is assigned to the aromatic

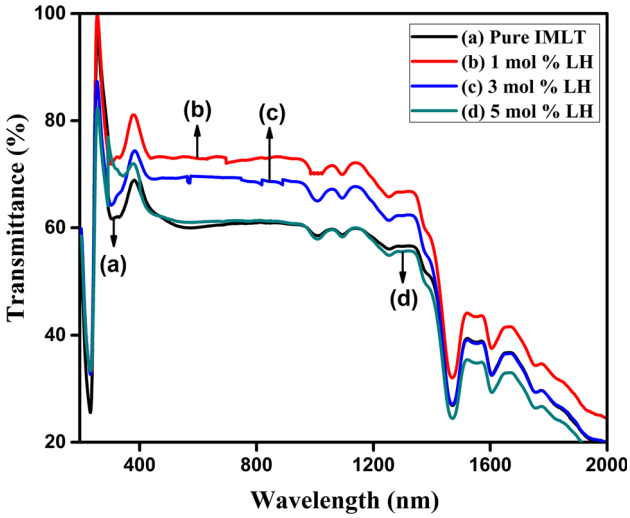

Fig. 6. UV–Vis-NIR transmission spectrum of the grown crystals.

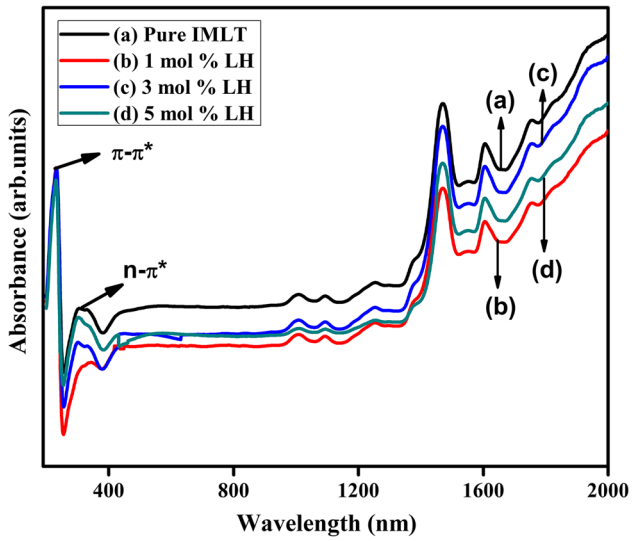

Fig. 7. UV–Vis-NIR absorption spectrum of the grown crystals.

Table III. The cut-off wavelength and optical band gap of the grown crystals

Crystal	Cut-off wavelength (nm)	Optical band gap E_g (eV)
Pure IMLT	234	4.72
1 mol.% L-histidine	229	4.89
3 mol.% L-histidine	230	4.85
5 mol.% L-histidine	233	4.79

heterocyclic structure of imidazole.[3] The 1 mol.% L-histidine-doped IMLT crystal is found to be much more transparent than all the other crystals. This is due to the good crystallinity of 1 mol.% L-histidine-doped IMLT crystal as compared to the all the other grown crystals, as explained in the PXRD analysis section. There may be an absence of solvent inclusions, which in turn increases the optical property by reducing the scattering centres as compared with the other grown crystals.[12] The cut-off wavelength of pure and 1 mol.% L-histidine-doped IMLT crystals are observed at 234 and 229 nm, respectively, which is summarized in Table III. It is also observed that doping till 1 mol.% increases the transparency of the IMLT single crystal in the entire visible and IR regions, and enables good optical transmission; this implies its suitability in UV tunable laser applications. In the absorption spectrum (Fig. 7), the high, intense peaks are observed at 231 nm and 317 nm, corresponding to the π–π^* and n–π^* transitions.[13–15] The value of the absorption coefficient was calculated using the following relations:

$$\alpha = -\frac{\ln T}{t} \tag{4}$$

$$\alpha = \frac{\ln \frac{1}{T}}{t} \tag{5}$$

$$\alpha = \frac{-2.303 \log T}{t} \tag{6}$$

where t is the thickness of the sample, T is the transmittance (%) and α is the absorption coefficient. The optical band gap energy of the grown crystals was calculated using the Tauc's plot (Fig. 8) by using the relation[14]

$$\alpha h\nu = A\left(h\nu - E_g\right)^n \tag{7}$$

where $h\nu$ is the photon energy, A is a constant, E_g is the optical energy band gap and n is the characteristic transition. The transition between the valence band and the conduction band can be either direct or indirect, and it can also be a forbidden transition. The transition number (n) is 1/2 for direct allowed transition, 2 for indirect allowed transition, 3/2 for direct forbidden transition and 3 for the indirect forbidden transition.[16] The value of n for pure IMLT crystal was found to be 2 as in the reported data, which confirms that the crystal exhibits indirect allowed transition;[3] i.e., the optical band gap of the pure IMLT crystal is an indirect bandgap in nature. Therefore, by rearranging the Tauc's plot relation, the following equation for the indirect allowed transition has been obtained:

$$\alpha h\nu = A\left(h\nu - E_g\right)^2 \tag{8}$$

$$(\alpha h\nu)^{\frac{1}{2}} = A\left(h\nu - E_g\right) \tag{9}$$

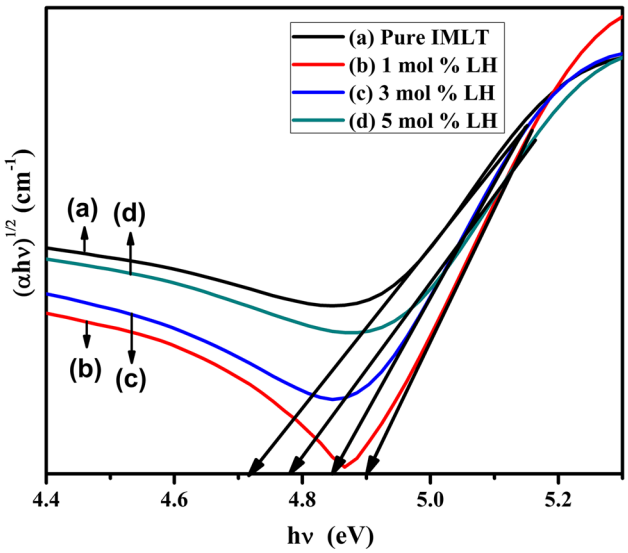

Fig. 8. Tauc's plot of $(\alpha h\nu)^{1/2}$ versus photon energy of the grown crystals.

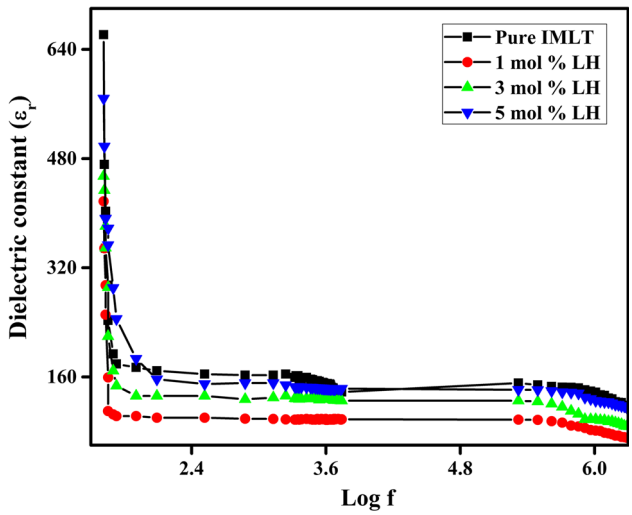

Fig. 9. Variation of dielectric constant as a function of frequency.

The optical band gap (E_g) values were calculated from $(\alpha h\nu)^{1/2}$ versus $h\nu$ and are also presented in Table III. The calculated optical band gap value of pure IMLT single crystal is 4.72 eV, and for 1 mol.% L-histidine-doped IMLT, it is 4.89 eV. Increase in the optical band gap value, the lower cut-off wavelength and an increase in the transparency range suggests that doping 1 mol.% L-histidine in IMLT crystal plays a vital role in improving the optical quality of the IMLT crystal.

Dielectric Studies

When a dielectric material is exposed to an external field, the positive charges align themselves in the direction of the electric field, and negative charges align against the applied electric field; therefore, there is a shift in the charge distribution which, in turn, gives rise to polarization. The dielectric response of the grown crystals gives the information about electro-optic property of the crystals; they are inter-related with each other. The grown crystals were cut and polished. The dimensions of the crystals were a surface area of 3 mm^2 and a thickness of 2 mm. Then the samples were coated with silver paste on either side to make them act like a parallel plate capacitor. The dielectric measurements of IMLT crystals and L-histidine-doped IMLT crystals were made using a Hioki 3532-50 LCR Hitester for different frequencies from 50 Hz to 5 MHz. The dielectric constant (ε_r) represents the amount of attenuation of the electric field in a material.

$$\text{dielectric constant,} \quad \varepsilon_r = \frac{Cd}{\varepsilon_0 A} \qquad (10)$$

where C is the capacitance, ε_0 is the permittivity of free space, d is the thickness of the grown crystal and A is the surface area of the crystal. Figure 9 shows the variation of the dielectric constant with the frequency for the grown crystals. The magnitude of the dielectric constant depends on the degree of polarization; i.e., the charge displacement in the crystals.[11] The larger value of the dielectric constant at a lower frequency is due to the contribution of all types of polarization; i.e., space-charge, ionic, dipole and electronic polarization mechanisms. However, each polarization mechanism has its own natural frequency and relaxation period. The space-charge polarization relaxes at a higher frequency and does not contribute to the net polarization.[3,12] Hence, the decrease in dielectric constant with an increase in frequency is observed in Fig. 9. This is due to the gradual disappearance of each polarization while increasing the frequency, and only the electronic polarization contributes to the higher frequencies. In general, as the frequency increases, the net polarization (the local displacement of dipoles) drops. Because, at low frequency, the dipoles can easily switch their alignment with the changing electric field. If the frequency increases, the dipoles cease to contribute and maintain phase with the field; this could also be a cause for the drop in the dielectric constant.[17] At low frequency, along with the four polarizations, the bound electrons and lattice vibrations also contribute to the high value of dielectric constant, but the space charge polarization is predominant.[18] The 1 mol.% L-histidine-doped IMLT crystal has the lower magnitude of dielectric constant at higher frequencies compared to the all the other grown crystals. Therefore, the power dissipation is relatively low, which implies that this crystal is well suited for microelectronic and NLO applications.[12,19] The dielectric constant decreases with

the increase in the frequency and becomes saturated beyond 3.5 Hz.

Dielectric loss ($\tan\delta$) can be calculated using the following relation

$$\tan\delta = \frac{\varepsilon''}{\varepsilon_0} \tag{11}$$

where $\varepsilon'' = \varepsilon_r \cdot D$.

D is the dissipation factor, and the dielectric loss at various frequencies is shown in Fig. 10. It shows that the dielectric loss decreases with the increase in frequency, similar to that of the dielectric constant.[20] The 1 mol.% L-histidine-doped IMLT crystal turns out to be a crystal of better optical quality with minimum defects, as evidenced by the lower magnitude of dielectric loss at higher frequencies, as observed in Fig. 10.

Etching Studies

The etching study conveys the growth features of the crystal.[21] Structural defects and crystal perfection can also be revealed by using etching studies. It is a powerful tool to analyze the quality of the crystal. The optical property of the crystal depends on the crystal perfection, and this affects the utility of the crystal. An optical microscope was used to study the morphology of the etch pits. In the present work, water was used as an etchant. Small crystals of about 2-mm thickness were employed for etching studies. The samples were immersed in the etchant for about 10 s for etching and then dried using tissue paper. The obtained features were examined using an optical microscope in the reflection mode, and the patterns are shown in Fig. 11a, b, c and d.

The patterns of the etch pits could be etch spirals, etch hillocks, or flat-bottomed pits that are developed by etching the surface.[22] Rectangular etch pits were observed for pure IMLT and L-histidine-doped IMLT crystals. The etch pits are the protrusions of the dislocation lines; they are formed due to the inclusions at the strain field surrounding the dislocation line. They are connected with the inclusions in the crystals, and these may distort the normal lattice arrangement that results in the lattice strain and mismatch in the crystal. In order to relax the strain and adjust the mismatch, dislocations are observed.[23] The addition of the dopant is compensated by the incorporation of the dopant in the etch pit morphology. The etch patterns show that the number of dislocations and the etch pits developed are reduced in 1 mol.% L-histidine-doped IMLT. Furthermore, increasing the etch time to 20 s decreases the size of the etch pit, but the pattern remains the same.

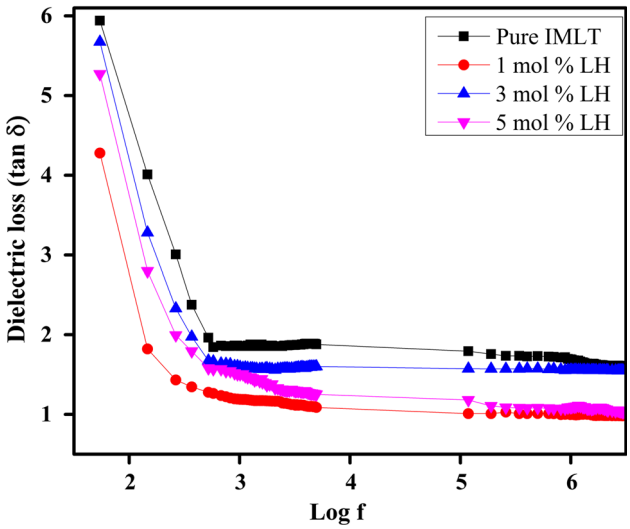

Fig. 10. Variation of dielectric loss as a function of frequency.

FTIR Analysis

Organic compound absorbs the electromagnetic energy in the infrared region of the spectrum, each peak in the spectrum represents the absorption of IR radiation at that frequency.[24] The functional groups present in the compound were confirmed by FTIR spectral analysis in the range of 400–4000 cm^{-1} by using KBr pellet technique, employing IR tracer-100 (Shimadzu). Figure 12 represents the FTIR spectrum of the grown crystals. The intense signal at 3151 cm^{-1} is due to the N–H stretches of the imidazole ring. The aromatic ring vibrations and their characteristic peaks were observed around 1202 cm^{-1} and are furnished in Table IV.

CHN Analysis

Carbon-hydrogen-nitrogen (CHN) analysis was carried out to confirm the chemical composition of pure IMLT and L-histidine-doped IMLT using the instrument Elementar Vario EL III CHNS analyser. The results of the analysis are compared, and they are presented in Table V. From Table V, it is observed that the experimental and theoretical values of carbon, hydrogen, and nitrogen elements agree with each other and confirms the formation of IMLT. The composition of carbon, hydrogen and nitrogen elements of the synthesized material has increased with increasing the dopant concentration. This confirms the incorporation of the L-histidine in the host lattice. Further on the basis of CHN analysis, the pure IMLT, 1 mol.%, 3 mol.% and 5 mol.% L-histidine-doped IMLT crystals molar ratios are found to be 1:0.2, 1:0.5 and 1:0.7, respectively. This ratio is based on the relative amounts of carbon, hydrogen and nitrogen elements present in the grown crystals.[25]

Z-Scan Analysis

The *Z*-scan technique is a reliable tool to characterize the third-order NLO parameters of the optical material. The magnitude and sign of the nonlinear absorption coefficient (β) and the nonlinear

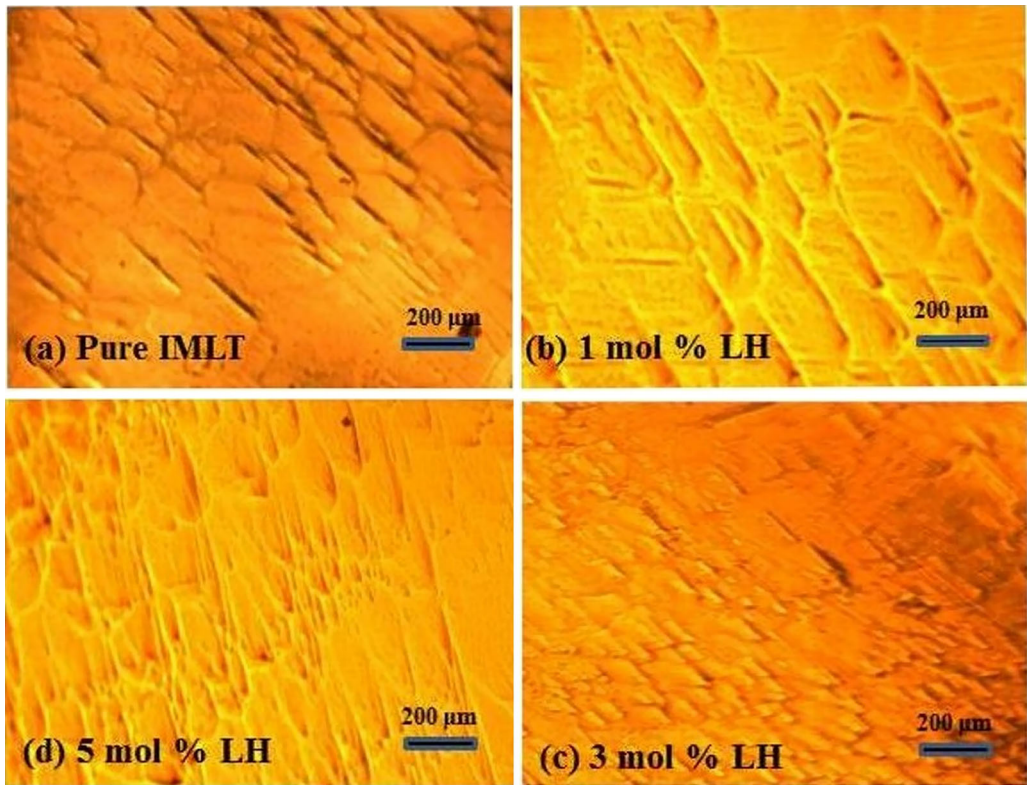

Fig. 11. Etch patterns of the grown crystals after etching for 10 s by water.

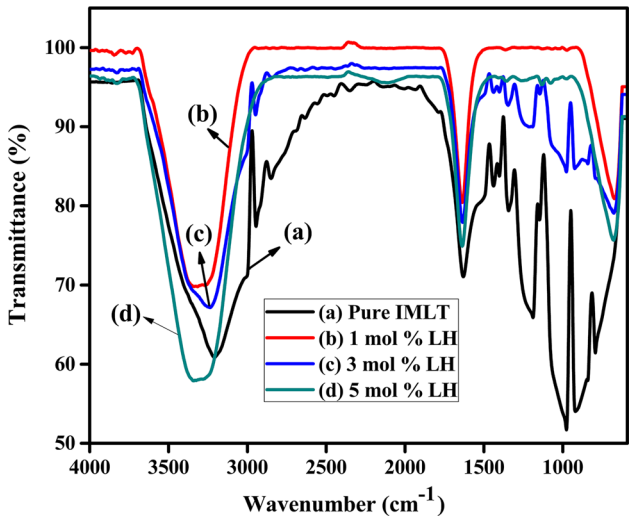

Fig. 12. FTIR spectrum of the grown crystals.

refractive index (n_2) of the material can be determined using the Z-scan method.[26] Z-scan technique employs two methods, closed- and open-aperture techniques. An intense laser beam using a continuous-wave, 532-nm, diode-pumped Nd:YAG Gaussian laser beam is focused through a convex lens on the optical material. The beam can induce a change in the refractive index of the material, which is proportional to the intensity of the beam (the Kerr effect); i.e., the intensity of the laser beam depends on the nonlinear refractive index and nonlinear absorption coefficient of the sample.[27] The total refractive index of the material is the sum of the linear refractive index (n_0) with no laser beam present and the product of the intensity of the beam and nonlinear refractive index of the material.

$$n = n_0 + n_2 I \tag{12}$$

A change in the refractive index can be positive or negative. The nonlinear medium can act as a lens and alters the focusing effect of the beam caused by the convex lens. The effect can be either self-focusing of the beam for a positive refractive index of the nonlinear medium or self-defocusing for the negative refractive index of the nonlinear medium.[15] The thickness of the sample should be less than that of the Rayleigh length (Z_R), $Z_R > L$.

$$Z_R = \frac{\pi \omega_0^2}{\lambda} \tag{13}$$

where λ is the wavelength of the laser beam and ω_0 is the beam waist diameter ($2\omega_0$). The nonlinear refractive index and the nonlinear absorption coefficient can be measured by moving the sample along the z-axis, which is along the direction of propagation of the laser beam. By placing the sample at the focal length (z =, 0) the normalized condition of the Z-scan is obtained. Then the sample is moved back

Table IV. FTIR spectral assignment of the grown crystals

Pure IMLT	1 mol.% L-histidine	3 mol.% L-histidine	5 mol.% L-histidine	Assignment of functional groups
–	3826	3875	3842	NH_3^+ asymmetric stretching of L-histidine
3209	3237	3341	3316	O–H stretching in the carboxyl group
2945, 2850	2948, 2843	2965, 2847	2968, 2835	C–H symmetric stretching vibration of carboxyl group
2350	2642	2109	2642	Presence of N–H functional group in the title compound
1631	1635	1638	1637	C=N vibration
1439	1438	1591	1590	C=O stretching vibration of carboxylate groups
1402	1402	1411	1412	CH bending vibration
1343, 1188	1346, 1211	1357, 1261	1348, 1203	Bending stretching of NH_4
1147	1145	1132	1102	C–C stretching of imidazole
1072	1050	1076	1048	CO–OH stretching vibrations of carboxylate groups
976	977	983	973	C–H out of plane; C–C symmetric stretching
920	924	983	983	C–C–N symmetric stretching
833	841	832	835	Symmetric stretch of the imidazole ring
793	768	767	762	CH_3 rocking
682	676	678	672	C–C out-of-plane ring deformation

Table V. CHN analysis of the grown crystals

Element	Pure IMLT (%)	Theoretical values (pure IMLT, %)	1 mol.% L-histidine (%)	3 mol.% L-histidine (%)	5 mol.% L-histidine (%)
C	38.62	38.50	38.93	39.02	39.16
H	4.40	4.5	4.48	4.50	4.57
N	12.67	12.8	12.78	12.83	12.86

and forth along the negative ($-z$) to the positive ($+z$) axis.[28] The corresponding transmitted intensity from the sample is received and analysed by the detector. In the closed-aperture technique, the intensity received depends on the aperture radius (r_a). The measurement starts from $-z$-axis, and the sample is then moved towards the focus and to the $+z$-axis, exposing it to the continuously varying laser intensity as it moves.

When the sample is close to the convex lens, the sample tends to focus or defocus the already focused beam depending on the negative or positive refractive index. When the sample reaches the focal length of the lens, the beam profile returns to its original one due to the thin lens approximation. When the sample is moved away from the focal length, the beam profile changes in its opposite manner. The self-defocusing behaviour of the sample is determined by the pre-focal transmittance peak followed by post-focal transmittance valley, indicating the negative index of refraction ($n_2 < 0$).[28] The self-focusing nature of the sample is determined by the pre-focal transmittance valley followed by post-focal transmittance peak, indicating the positive index of refraction ($n_2 > 0$).[28] The difference between the transmittance peak and transmittance valley is given by:

$$\Delta T_{p-v} = 0.406(1-S)^{0.25}|\Delta\varphi| \tag{14}$$

where $\Delta\varphi$ the on-axis phase shift at the focus, S is the linear transmittance aperture and is calculated using the following relation

$$S = 1 - \exp\left(\frac{-2r_a^2}{\omega_a}\right) \tag{15}$$

The third-order nonlinear refractive index is related to the on-axis phase shift by

$$n_2 = \frac{\Delta\varphi}{kI_0L_{eff}}\left(\frac{m^2}{W}\right) \tag{16}$$

where $k = \frac{2\pi}{\lambda}$, I_0 is the intensity of the laser beam at the focus (z = 0) and $L_{eff} = \frac{1-\exp(-\alpha L)}{\alpha}$ is the effective thickness of the sample. The closed-aperture transmittance data for pure and L-histidine-doped IMLT is given in Fig. 13a. The peak followed by a valley confirms the self-defocusing nature of the IMLT crystals, indicating the negative refractive index.

The nonlinear refractive index (n_2) and the linear refractive index (n_0) values of pure and L-histidine-doped IMLT crystals are given in Table VI. The negative refractive index value predicts that the

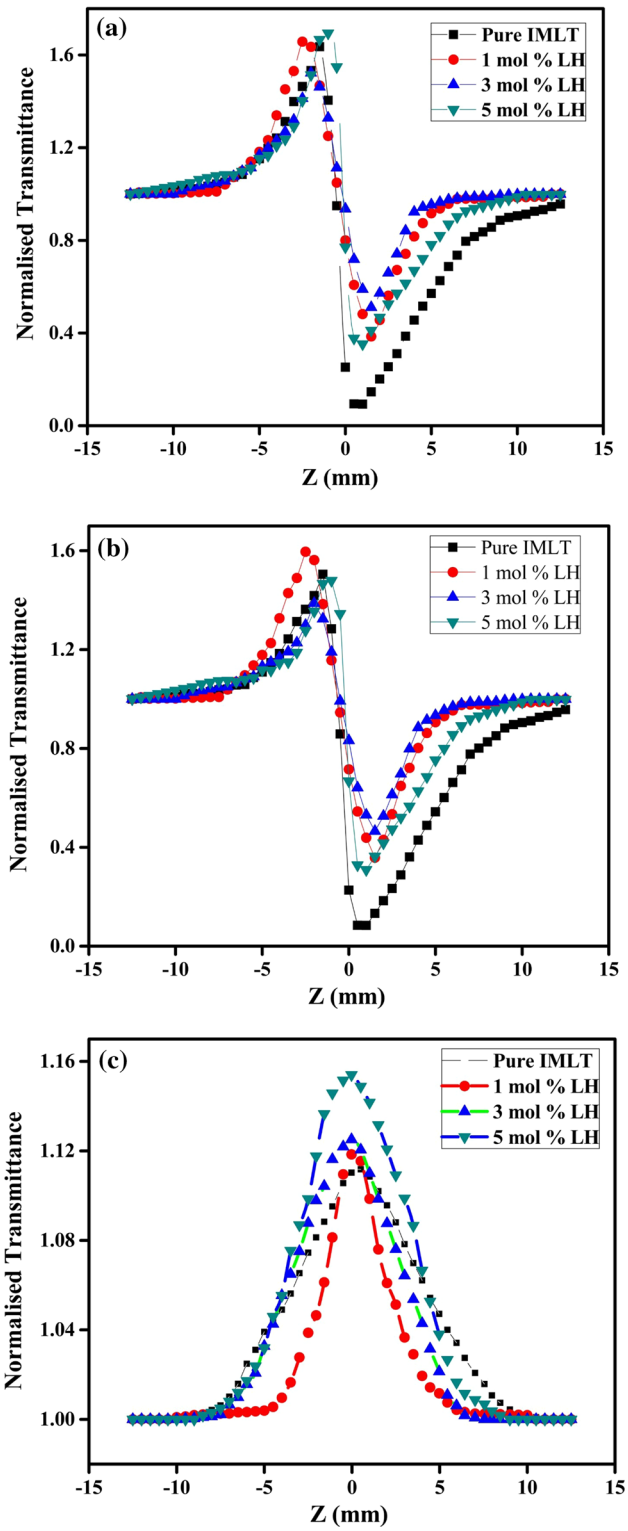

Fig. 13. (a) Closed-aperture *Z*-scan data. (b) Ratio of closed-aperture and open-aperture *Z*-scan data. (c) Open-aperture *Z*-scan data of the grown crystals.

IMLT crystals can have significant application in optical night-sensor devices. The ratio of closed- and open-aperture *Z*-scan data represents the pure nonlinear refraction[26] and is shown in Fig. 13b. The open aperture *Z*-scan data provides the nonlinear absorption coefficient (β),

$$\beta = \frac{2\sqrt{2}\Delta T}{I_0 L_{eff}} \left(\frac{\mathrm{m}}{\mathrm{W}}\right) \tag{17}$$

where ΔT is the one peak or valley value in the open-aperture *Z*-scan data. The value of β can be negative or positive, which is saturable absorption for negative and reverse saturable absorption for positive. The grown crystals were subjected to open-aperture *Z*-scan technique, and the obtained data is shown in Fig. 13c. The data estimated by open-aperture method confirms the saturable absorption behaviour and the negative nonlinear absorption coefficient of the grown crystals. The real and imaginary parts of the third-order nonlinear optical susceptibility were calculated using the following relations:

$$R_e\left(\chi^{(3)}\right)(\mathrm{esu}) = \frac{10^{-4}\varepsilon_0 C^2 n_0^2 n_2}{\pi} \left(\frac{\mathrm{cm}^2}{\mathrm{W}}\right) \tag{18}$$

$$I_m\left(\chi^{(3)}\right)(\mathrm{esu}) = \frac{10^{-2}\varepsilon_0 C^2 n_0^2 \lambda \beta}{4\pi^2} \left(\frac{\mathrm{cm}}{\mathrm{W}}\right) \tag{19}$$

where ε_0 is the vacuum permittivity $\left(8.8518 \times 10^{-12}\left(\frac{\mathrm{s}}{\mathrm{m}}\right)\right)$, C is the velocity of light (3×10^8 m/s), n_0 is the linear refractive index of the sample and λ is the wavelength of the laser beam (532 nm). The third-order nonlinear optical susceptibility values of the crystals are calculated by

$$\chi^{(3)} = \sqrt{\left(R_e(\chi^{(3)})\right)^2 + \left(I_m(\chi^{(3)})\right)^2}\,\mathrm{esu} \tag{20}$$

1 mol.% L-histidine-doped IMLT has the highest nonlinear optical susceptibility, which implies enhanced delocalization of π-electrons cloud result in a high polar nature, suggesting its suitability for sensor devices and optical limiting.

CONCLUSIONS

Pure IMLT and L-histidine-doped IMLT crystals were grown by slow evaporation method. The cell parameters and monoclinic crystal system of the grown crystals were confirmed using powder X-ray diffraction analysis. The shift in the diffraction peaks upon increasing the dopant concentration shows the incorporation of dopant in the crystal lattice. The dislocation density and strain were calculated using the Debye–Scherrer method which describes the superior property of 1 mol.% L-histidine-doped IMLT crystals. The 1 mol.% L-histidine-doped crystal appears to be highly

Table VI. Nonlinear optical parameters of the grown crystals

Sample	n_2 10^{-8} cm^2/W	β 10^{-4} cm/W	n_0	Re $\chi^{(3)}$ 10^{-6} esu	Im $\chi^{(3)}$ 10^{-6} esu	$\chi^{(3)}$ 10^{-6} esu
Pure IMLT	8.34	0.09	1.32	3.67	0.58	3.71
1 mol.% L-histidine	6.64	0.09	1.57	4.16	0.56	4.19
3 mol.% L-histidine	6.82	0.13	1.41	3.45	0.79	3.54
5 mol.% L-histidine	5.08	0.10	1.04	1.39	0.60	1.51

transparent. This was confirmed using UV–Vis-NIR spectral studies. The cut-off wavelength was found to decrease in 1 mol.% L-histidine-doped IMLT crystal. The band gap was calculated from the Tauc's plot as 4.72 eV and 4.89 eV for pure IMLT and 1 mol.% L-histidine-doped IMLT crystals. The etching study reveals the growth process and growth mechanisms of pure and doped IMLT crystals and the decrease in EPD in 1 mol.% L-histidine-doped IMLT crystals. The dielectric study reveals a decrease in the dielectric constant and dielectric loss while increasing the dopant concentration till 1 mol.% L-histidine. The CHN analysis conveys the percentage of carbon, hydrogen and nitrogen in pure and L-histidine-doped IMLT crystals, and the increase in the percentage of C, H and N elements while increasing the dopant concentration was confirmed. The *Z*-scan technique reveals the 1 mol.% L-histidine-doped IMLT crystal has a relatively larger NLO susceptibility, which is necessary for NLO device applications. Through the performed characterization studies, we confirm that the 1 mol.% L-histidine-doped IMLT crystal possesses superior quality compared to pure and other doped crystals, favouring their utilization in NLO device applications.

ACKNOWLEDGMENTS

One of the authors (P. Dhivya) is thankful to the TEQIP-III, PSG College of Technology (TEQIP/NoA/17 dated 25.11.2017) for the financial assistance to carry out this work.

REFERENCES

1. N. Pattanaboonmee, P. Ramasamy, R. Yimnirun, and P. Manyum, *J. Cryst. Growth* 314, 196 (2011).
2. M. Prakash, D. Geetha, M. Lydia Caroline, and P.S. Ramesh, *Spectrochim. Acta A* 83, 461 (2011).
3. N. Elavarasu, S. Karuppusamy, S. Muralidharan, M. Anantharaja, and R. Gopalakrishnan, *Opt. Mater.* 46, 141 (2015).
4. C. Ji, T. Chen, Z. Sun, Y. Ge, W. Lin, J. Luo, Q. Shi, and M. Hong, *CrystEngComm* 15, 2157 (2013).
5. S. Suresh, *J. Electron. Mater.* 45, 5904 (2016).
6. T. Prasanyaa, M. Haris, V. Mathivanan, M. Senthilkumar, T. Mahalingam, and V. Jayaramakrishnan, *Mater. Chem. Phys.* 147, 433 (2014).
7. S.M. Azhar, M. Anis, S.S. Hussaini, S. Kalainathan, M.D. Shirsat, and G. Rabbani, *Opt. Laser Technol.* 87, 11 (2017).
8. A. Kumaresh, R. Arun Kumar, M. Arivanandhan, and Y. Hayakawa, *J. Cryst. Growth* 401, 874 (2014).
9. K. Meena, K. Muthu, V. Meenatchi, M. Rajasekar, G. Bhagavannarayana, and S.P. Meenakshisundaram, *Spectrochim. Acta A* 124, 663 (2014).
10. P. Singh, M. Hasmuddin, M. Shakir, N. Vijayan, M.M. Abdullah, V. Ganesh, and M.A. Wahab, *Mater. Chem. Phys.* 142, 154 (2013).
11. P. Singh, M. Hasmuddin, N. Vijayan, M.M. Abdullah, M. Shakir, and M.A. Wahab, *Optik* 124, 1609 (2013).
12. A. Mohd, G.G. Muley, M.D. Shirsat, and S. Hussaini, *Cryst. Res. Technol.* 50, 372 (2015).
13. K. Mohanraj, D. Balasubramanian, and N. Jhansi, *Opt. Laser Technol.* 96, 318 (2017).
14. G. Vadivelan, V. Murugesan, M. Saravanabhavan, and M. Sekar, *Optik* 140, 571 (2017).
15. P. Karuppasamy, M. Senthil Pandian, P. Ramasamy, and S. Verma, *Opt. Mater.* 79, 152 (2018).
16. P. Karuppasamy, M. Senthil Pandian, P. Ramasamy, and S.K. Das, *Optik* 156, 707 (2018).
17. A. Senthil and P. Ramasamy, *J. Cryst. Growth* 312, 276 (2010).
18. M.R. Jagadeesh, H.M. Suresh Kumar, and R. Ananda Kumari, *Optik* 126, 4014 (2015).
19. D. Sathya and V. Sivashankar, *Optik* 126, 5873 (2015).
20. T.P. Srinivasan, R. Indirajith, and R. Gopalakrishnan, *J. Cryst. Growth* 312, 542 (2010).
21. V. Sivasubramani, M. Senthil Pandian, K. Boopathi, and P. Ramasamy, *Mater. Res. Innov.* 22, 128 (2018).
22. F. Akhtar and J. Podder, *J. Cryst. Process Technol.* 1, 55 (2011).
23. M. Senthil Pandian, N. Balamurugan, G. Bhagavannarayana, and P. Ramasamy, *J. Cryst. Growth* 310, 4143 (2008).
24. G. Bhuvaneswari, L. Guru Prasad, and N. Prabavathi, *Optik* 166, 307 (2018).
25. M. Krishna Mohan, K. Jagannathan, S. Ponnusamy, and C. Muthamizhchelvan, *J. Phys. Chem. Solids* 72, 1273 (2011).
26. P.V. Dhanaraj, N.P. Rajesh, J. Kalyana Sundar, S. Natarajan, and G. Vinitha, *Mater. Chem. Phys.* 129, 457 (2011).
27. T.C. Sabari Girisun, S. Dhanuskodi, and G. Vinitha, *Mater. Chem. Phys.* 129, 9 (2011).
28. P. Karuppasamy, M. Senthil Pandian, P. Ramasamy, and S. Verma, *Opt. Mater.* 79, 152 (2018).